JOURNAL OF GEOPHYSICAL RESEARCH, VOL. 103, NO. A3, PAGES 4303–4314, MARCH 1, 1998

Freja and ground-based analysis of inverted-V events

H.U. Frey,[1,2] G. Haerendel,[1] J.H. Clemmons,[1,3] M.H. Boehm,[1,4] J. Vogt,[1]
O.H. Bauer,[1] D.D. Wallis,[5] L. Blomberg,[6] and H. Lühr[7,8]

Abstract. During two campaigns, ground-based auroral observations were performed in coordination with Freja. The high temporal and spatial resolution of the satellite instruments as well as the real-time recording with a stereoscopic camera system from the ground enabled detailed comparison of small- and large-scale optical phenomena with particle and field data measured by the satellite. Three passes of the satellite over inverted-V auroral arcs and over precipitation regions with strong field-aligned electron spectra are investigated. Brightness modulations within auroral arcs coincide with modulations of primary electron fluxes. The dynamics of small-scale structures within arcs as well as the proper motion of arcs are analyzed and compared with electric fields measured by the satellite and with BARS radar measurements. Energy fluxes independently determined from the ground and from the satellite are used to calculate the field-aligned conductance. The results agree with predictions of the kinetic theory of the mirror force, if we allow for variations of the density and thermal energy of the electrons in the source region of the magnetosphere. Detailed comparison of electron spectra and electric and magnetic field perturbations provide evidence of different acceleration mechanisms for the electrons, electrostatic acceleration inside inverted-V's, and wave acceleration in transient regions.

1. Introduction

Since the very early publications by *Frank and Ackerson* [1971] and *Gurnett* [1972] inverted-V structures in electron energy-time spectrograms are a well accepted signature of electron precipitation into the auroral zone creating auroral arcs [*Gurnett and Frank,* 1973; *Mozer et al.,* 1980; *Chiu et al.,* 1983; *McFadden et al.,* 1990; *Sakanoi et al.,* 1995]. Because of low data rates and high perpendicular velocities resulting in low spatial and time resolution, the first studies investigated broad structures of 200-300 km latitudinal width. Narrow auroral arcs of $\approx$ 10 km width were studied by rockets with slower velocities and higher telemetry rates. An important step to close the gap between these situations was the launch of the Swedish/German scientific satellite Freja in 1992. The spatial resolution of some instruments equals that of sounding rockets, while the time resolution is higher than that of most previous measurements. Thus, with this satellite, not only broad but also narrow structures down to $\approx 1-5$ km could be studied [*Boehm et al.,* 1994a].

One still existing difficulty with the interpretation of satellite measurements is the separation of spatial and temporal variations. The combination with ground-based observations cannot solve this difficulty but can provide much better limits. For this purpose and in continuation of earlier radar supported campaigns on the physics of auroral arc formation and dynamics [*Haerendel et al.,* 1993; *Frey et al.,* 1996a] the Max-Planck-Institute for Extraterrestrial Physics (MPE) developed a low-light-level CCD camera system with the aim to record high-time-resolution and wide-angle stereo images of the aurora during passes of the Freja satellite. This system was used during campaigns in February/March 1993 and this paper summarizes the results of the investigation of inverted-V events. On the basis of previously published first results [*Haerendel et al.,* 1994; *Frey et al.,* 1996b], one more event will be presented, the methods of data analysis will be extensively discussed, and the data will further be investigated with emphasis on the dynamics and the creation of auroral arcs.

While the energy-time spectrograms of inverted-V's generally show slowly varying and isotropic electron flux, there is frequently considerable energy fluctuation and fine structure embedded. *Chiu et al.* [1983] interpreted this in terms of spatial modulations of the basic U-shaped potential structure in the acceleration region. In this paper we compare observed motions of auroral arcs and fine structures with the corresponding

[1]Max-Planck-Institut für Extraterrestrische Physik, D-85740 Garching, Germany.
[2]now at SSL, University of California, Berkeley.
[3]now at Goddard Space Flight Center, Greenbelt, Maryland.
[4]now at Lockheed Martin, Palo Alto, California.
[5]Hertzberg Institute of Astrophysics, Ottawa, Canada.
[6]Royal Institute of Technology, Stockholm, Sweden.
[7]Institut für Geophysik und Meteorologie, Braunschweig, Germany.
[8]now at GeoForschungszentrum, Potsdam, Germany.

Paper number 97JA02259.
0148-0227/98/97JA-02259$09.00

electric fields in the ionosphere. We demonstrate the close correspondence between optical emission and particle flux, evaluate the field-aligned conductance, and compare experimental results with theoretical predictions. Furthermore, we compare the electromagnetic and particle energy flux measured by the satellite in different regions within the auroral oval and determine whether these regions are controlled by the ionosphere or magnetosphere and whether the electrons are mainly accelerated by electrostatic fields or by waves.

2. Instrumentation and Data Analysis

The Swedish/German scientific satellite Freja was launched into an orbit with 63° inclination. The F1 electric field instrument measures the potential difference between opposing probes on 10-m booms in the spin plane. Measurements with a rate of 768 samples per second are performed in the dynamic range of ±1 V/m [*Marklund et al.*, 1994]. The F2 triaxial fluxgate magnetometer [*Zanetti et al.*, 1994] measures 128 vector samples per second. The F7 two-dimensional electron spectrometer [*Boehm et al.*, 1994b] consists of a top-hat-type electrostatic analyzer to measure the full electron distribution function from ≈ 20 eV to 25 keV at 32-ms time resolution and in 32 directions simultaneously.

Field-aligned current densities were calculated from the Freja magnetometer data assuming the current to be located in sheets aligned along the background magnetic field $\mathbf{B}_0$ (IGRF 90-95 model). First, time intervals were selected where sheet-like structures may exist, i.e., linear sections in the magnetogram and the magnetic hodogram. Second, the orientation of the current sheet normal vector $\mathbf{n}$ is calculated with a minimum variance analysis similar to the method described by *Sonnerup and Cahill* [1967], but in our case the covariance matrix is just 2×2 because only the directions perpendicular to the background magnetic field are considered. The technique is based on the assumptions that the sheets are sufficiently extended, stationary, and the current density inside the sheet is homogeneous. The ratio $\lambda_{min}/\lambda_{max}$ of the eigenvalues of the covariance matrix can be used to test the first assumption. Finite geometry effects on the minimum variance technique were discussed in detail by *Fung and Hoffman* [1992]. In general, data from a single satellite do not allow for a test of the stationarity assumption, but the pattern of the calculated current sheets along the orbit may serve as a consistency check. The homogeneity assumption can be tested with the help of the goodness-of-fit parameters of a linear regression. Then, the sheet width Δs is calculated with the satellite velocity component normal to the sheet orientation ($v_n = \mathbf{n} \cdot \mathbf{v}$) and the time interval Δt with

$$\Delta s = \int_{\Delta t} v_n dt \approx v_n \Delta t. \quad (1)$$

Finally, the current density $j_\parallel$ is calculated from the gradients in the perturbation magnetic field $\mathbf{B}_\perp$ with the help of Ampére's law

$$j_\parallel = \frac{1}{\mu_o} \frac{(\mathbf{n} \times \mathbf{B}_\perp)}{\Delta s} \cdot \frac{\mathbf{B}_0}{B_0}. \quad (2)$$

The electric field is measured within the spin plane of the satellite. A full vector description of the electric field was performed with the assumption that there is no electric field component along the magnetic field at the position of the satellite. Thus, after calculation of the spin axis orientation and local magnetic field the full electric field vector was calculated with $\mathbf{E} \cdot \mathbf{B} = 0$. Transformation from the satellite to ionospheric altitude was performed under the assumption of field continuity and taking into account the mapping along dipole field lines [*Borovsky*, 1993]. For the comparison with ground-based observations the electric field vector was decomposed into the components pointing to geographic north, east, and downward.

Additionally, the electric field at Freja altitude was rotated into a field-aligned coordinate system with the Z axis pointing along the background field and the Y axis pointing eastward. In this coordinate system the electric field as well as the perpendicular magnetic field are lying in the X-Y plane. Note that this coordinate system differs from the system described above.

The MPE ground-based optical equipment consisted of two image-intensified CCD-cameras with a maximum spectral sensitivity at 470-nm wavelength [*Frey et al.*, 1996c]. Both cameras were equipped with an all-sky lens with a speed of f/D=1:1.0. Out of the whole field of view the cameras used the central part of 86° × 64°. A filter stripe with three positions enabled use of different interference filters. Real-time imaging with a frame rate of 25 frames per second was performed most of the time. Exact timing of the cameras was possible with integrated GPS receivers.

The cameras operated from two sites near Gillam, Manitoba (Kettle at 265.360°E, 56.376°N; Limestone at 265.877°E, 56.510°N) separated by a distance of 35 km. The geometry of the system enabled stereoscopic observations with the aim of altitude and position determination. By absolute calibration of the cameras at different wavelengths the intensities in image pixels could be converted into absolute brightnesses after background subtraction and correction for image inhomogeneities and taking into account filter transmission, atmospheric extinction, and transmission of the all-sky optics [*Frey et al.*, 1996c].

A direction through local magnetic zenith and perpendicular to the mean arc elongation was defined and the position of the arc determined along this line. The arc brightness was determined at the intersection with this line, though this was not always the maximum brightness along the whole arc. The height of the arcs could not always be determined at this line because common structures within the images of the two cameras had to be identified for the triangulation, but we did it as often as possible.

Additionally, data of the Canadian Auroral Network for the OPEN Program Unified Study project (CANOPUS) instruments are used [*Grant et al.*, 1992].

3. Observations

3.1. March 18, 1993

During orbit 2152 on March 18, 1993, Freja passed the observation point from geographic northwest to

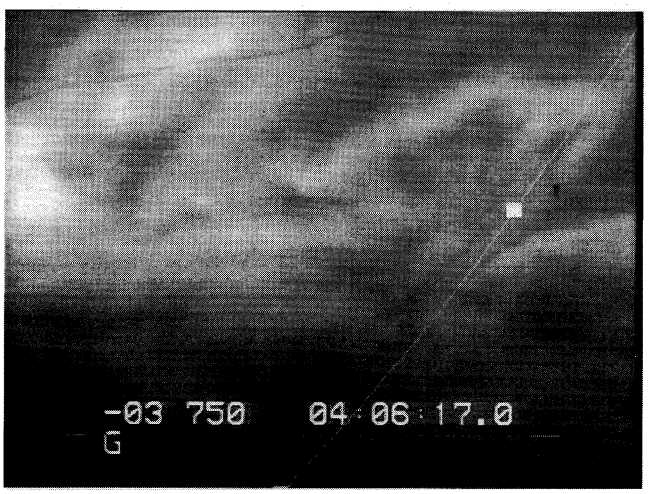

Figure 1. Auroral image taken on March 18, 1993, by the MPE CCD-camera with the track and the momentary conjugate point to Freja (white square).

southeast. Between 0406:00 and 0406:40 UT (2055 MLT) the conjugate points at 100 km altitude were visible in our camera's field of view with a maximum elevation of 76° (Figure 1).

Fifteen minutes before the Freja passage an auroral arc slowly moved southward. This arc showed a rayed structure together with the onset of Pi 2 pulsations when a breakup occurred, followed by a westward traveling surge passing overhead Gillam at 0401 UT. The original arc brightened and widened. During the Freja pass the equatorward part of that wide arc ($\approx$ 200 km in geomagnetic north-south direction) was in the field of view of our cameras with brightness patterns moving westward with velocities between 1.3 and 2.8 km/s.

The F1 experiment measured homogeneous electric fields of about 20 mV/m pointing north in the Gillam area, which is consistent with BARS radar data of a westward ionospheric plasma drift with velocities between 300 and 500 m/s (not shown).

Between 0404:40 and 0405:00 UT the F7 experiment measured a dominant flux of field aligned electrons of 3 mW/m^2 (Figure 2). Between 0405:20 and 0406:40 a typical broad inverted-V structure could be seen in the electron data creating energy fluxes of 7.0 mW/m^2.

The F2 magnetic field data (not shown) are dominated by downward field-aligned current sheets north of Gillam and a 260 ± 30 km thick upward current sheet of -0.42 ± 0.05 μA/m^2 overhead which belongs to the visible thick arc.

3.2. March 20, 1993

On March 20, 1993 (orbit 2178), Freja passed Gillam at 0320 UT (2010 MLT) during weakly disturbed geomagnetic conditions, about 90 min before a substorm. An eastward electrojet south of Gillam caused a $\Delta B_x \approx$ 35 nT disturbance of the local magnetic field which decreased between 0230 and 0330 UT when the BARS radar (Figure 3) determined the southward motion of the eastward electrojet. At 0305 UT the westward electrojet became dominant at Fort Churchill.

The all-sky cameras at Rabbit Lake and at Gillam showed a broad arc system spanning the whole sky from northwest to southeast overhead of both observation sites (Figure 4). South of the arc there was diffuse aurora. North of it, a region with very low auroral emission separated this arc from another arc over the Fort Churchill area which became visible after 0315 UT. The arc over Gillam moved slowly to the south. The northern arc moved to the north, changed very rapidly, and showed many brightness patterns and an unstable structure. After 0335 UT the northern arc left the field of view of the Gillam meridian scanning

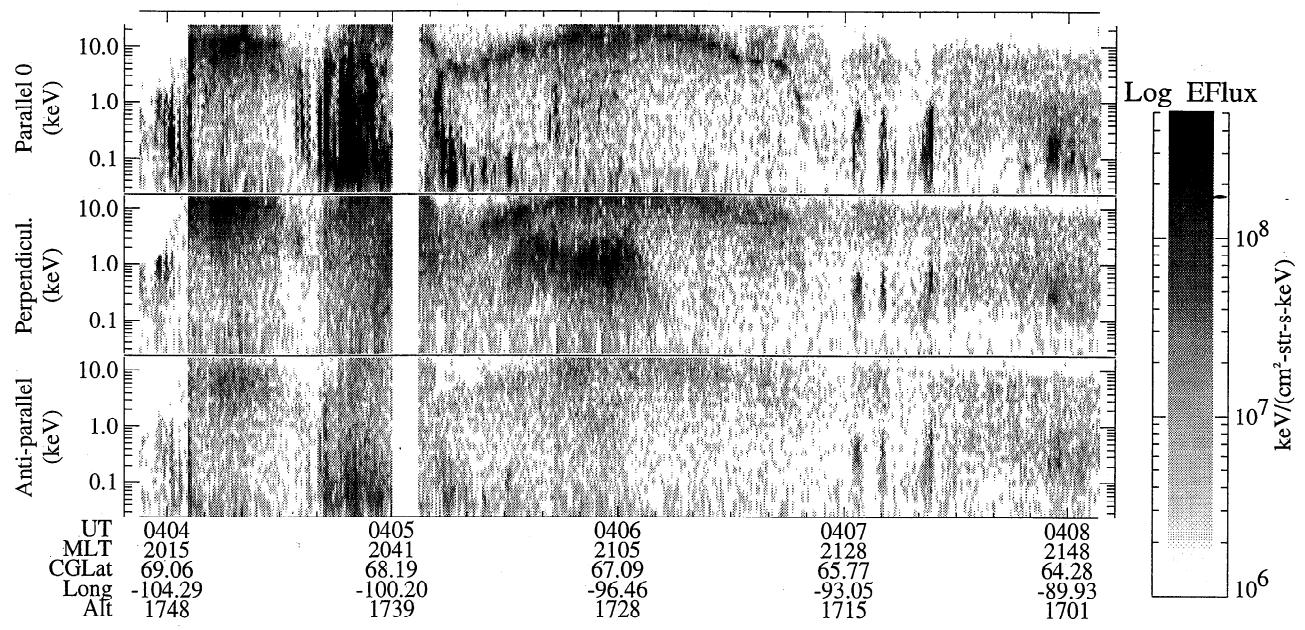

Figure 2. Freja electron spectrometer data from March 18 in the parallel, the perpendicular, and the anti-parallel channel.

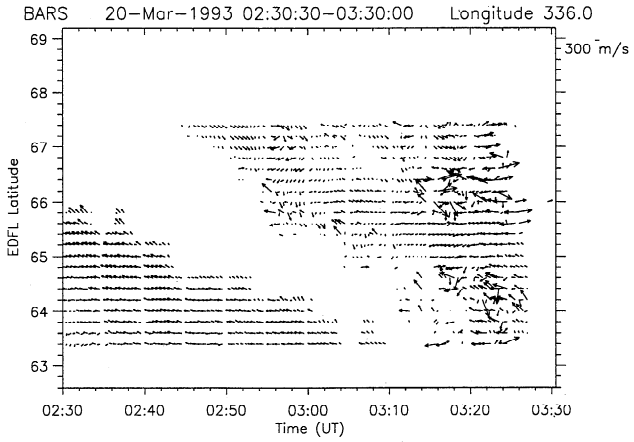

Figure 3. Time sequence of plasma drifts measured by the BARS radar on March 20 at constant eccentric dipole field line (EDFL [*Grant et al.*, 1992]) longitude of 336.0°. The EDFL latitude of Gillam is 63.88° and of Fort Churchill 66.27°.

photometer which means that it was more than 450 km further north. The enhanced electron precipitation due to the northern arc coincided with a small negative excursion of the horizontal local magnetic field component at Fort Churchill and with a localized perturbation of the direction and velocity of plasma flow in the ionosphere around 0315 UT (Figure 3). About 5 min later, the horizontal magnetic field component in Eskimo Point decreased by $\Delta B_x = -90$ nT. Thus the northward moving arc coincided with the flow reversal region separating eastward electrojet over Gillam from westward electrojet between Fort Churchill and Eskimo Point.

The main arc showed motions of brightness patterns to the east in the center of the arc with velocities increasing from 0.7 to 1.5 km/s, and a parallel fold system about 8 km south of the eastward drifting one, moving westward with similar velocities of 1.0 to 1.5 km/s.

Between 0308 and 0322 UT twenty current sheet structures could be identified in the Freja magnetometer data (Figure 5). Some of them belong together and represent elongated current sheets traversed by Freja twice (section 4), and some others represent the inhomogeneous current within one sheet. They very clearly show the location of the auroral oval (Figure 6). Freja entered the dominant arc far in the west at 0311:51 UT (Figure 7). The thickness of the current sheet with a mean current density of -1.3 ± 0.1 μA/m^2 was 180 km at Freja altitude. South of it (measurements around 0311 and 0321 UT) we find weak auroral precipitation of the diffuse aurora. After a region with very low electron precipitation Freja entered the region of flow reversal at 0315:22 UT with a downward directed current sheet of 19 ± 2 km thickness and a current density of 7 ± 1 μA/m^2. The arc in the north is the optical signature of several precipitation structures which Freja crossed between 0315:35 and 0318:18 UT and which caused a mixture of temporal and spatial changes in the electron spectrogram. During that time the analysis of the covariance matrix did not support the identification of current sheets, most probably because the assumption of extended sheets failed. The

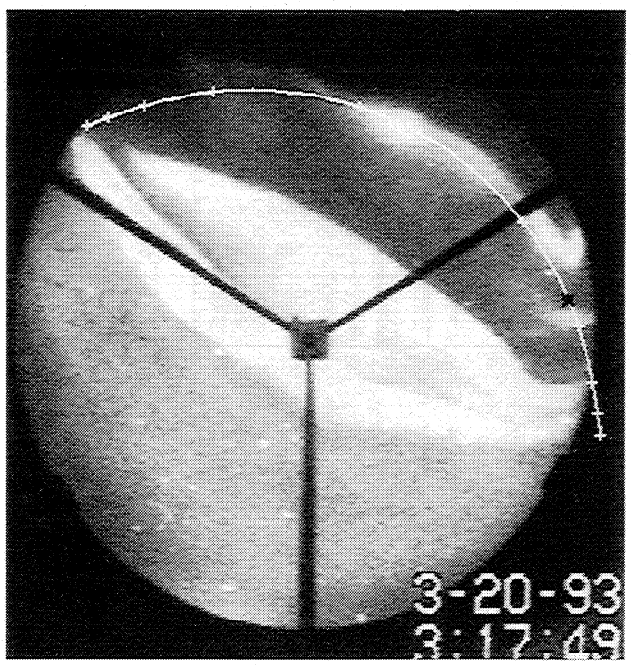

Figure 4. Pass of Freja over Rabbit Lake between (left) 0312:00 UT from west and (right) 0321:00 to southeast on March 20. The conjugate points at 125 km altitude and 1 min time steps are marked with a plus and the position of Freja with an asterisk.

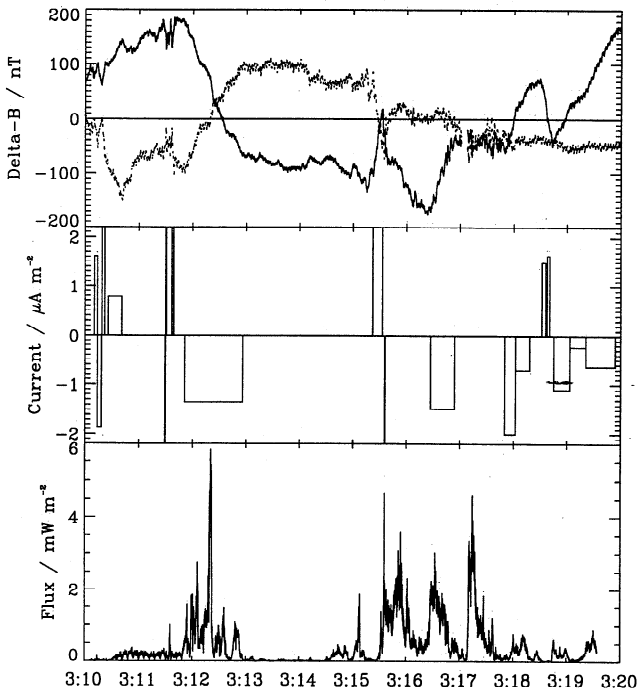

Figure 5. Current density derived from the local magnetic field perturbations (ΔB_x, dotted line; ΔB_y solid line)and energy flux (downward is positive) derived from the electron spectrogram for the Freja orbit on March 20.

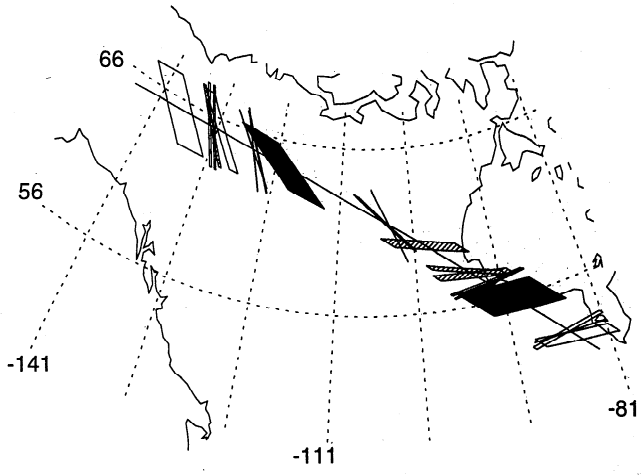

Figure 6. Projection of the Freja measured current sheets to the magnetic foot points along the satellite pass. The dark sheets belong to the inverted-V auroral arc, and other upward field-aligned current sheets are hatched.

optical dark gap between the arcs belongs to downward current sheets. Between 0318:45 and 0319:54 UT Freja entered the dominant arc overhead Gillam which represents three substructures with a mean current density of $-0.54\ \mu A/m^2$.

3.3. February 22, 1993

During orbit 1835 on February 22, 1993, Freja passed the Gillam area at 0410 UT (2050 MLT) west of the observation site from southwest to northeast (Figure 8). There was a small substorm around 0300 UT, but during the Freja pass the geomagnetic field was in the recovery phase.

From 0353 till 0415 UT the dynamics of the aurora was analyzed in detail (Figures 9 and 10). At 0353 UT an arc (further referred to as "first") could be seen in the northern part of the images and it moved to the south with a constant speed of 210 m/s. At 0354:20 UT another arc ("second") of equal brightness appeared 34 km south of the first one and moved to the south with 260 m/s. At 0356:00 UT the first arc disappeared, the second arc stopped moving, and during the following 30 s it increased brightness, and the altitude of maximum light emission decreased from about 120 to 100 km. After 0356:40 UT it rapidly moved to the south with an increase of altitude and a decrease of brightness. At that time a new arc ("third") appeared north of the second one with equal brightness and altitude of about 120 km.

The third arc moved to the south with 125 m/s until it stopped at 0357:40 UT, decreased altitude, did not move very much (7 m/s), and the brightness decreased again after the maximum at 0359:40 UT. Unfortunately, there are only images from one camera between 0357:50 and 0400:30 UT due to tape exchange during observation. Thus triangulation is impossible during that time. At 0400:50 UT a new arc ("fourth") could be identified 26 km south of the third one. The arcs had equal brightness and altitude and with a decrease of brightness both arcs moved to the south at 190 m/s, meanwhile increasing altitude up to 120-130 km. At 0406 UT the fourth arc became dominant, the next arc ("fifth") appeared 27 km south of it, and with increasing brightness and decreasing altitude it stopped moving (18 m/s). At 0408 UT the brightness decreased and the velocity increased again (100 m/s) until the fifth arc became dominant at 0409 UT.

The fifth arc stopped southward motion at 0410:40 UT (18 m/s), increased brightness until 0411:30 UT,

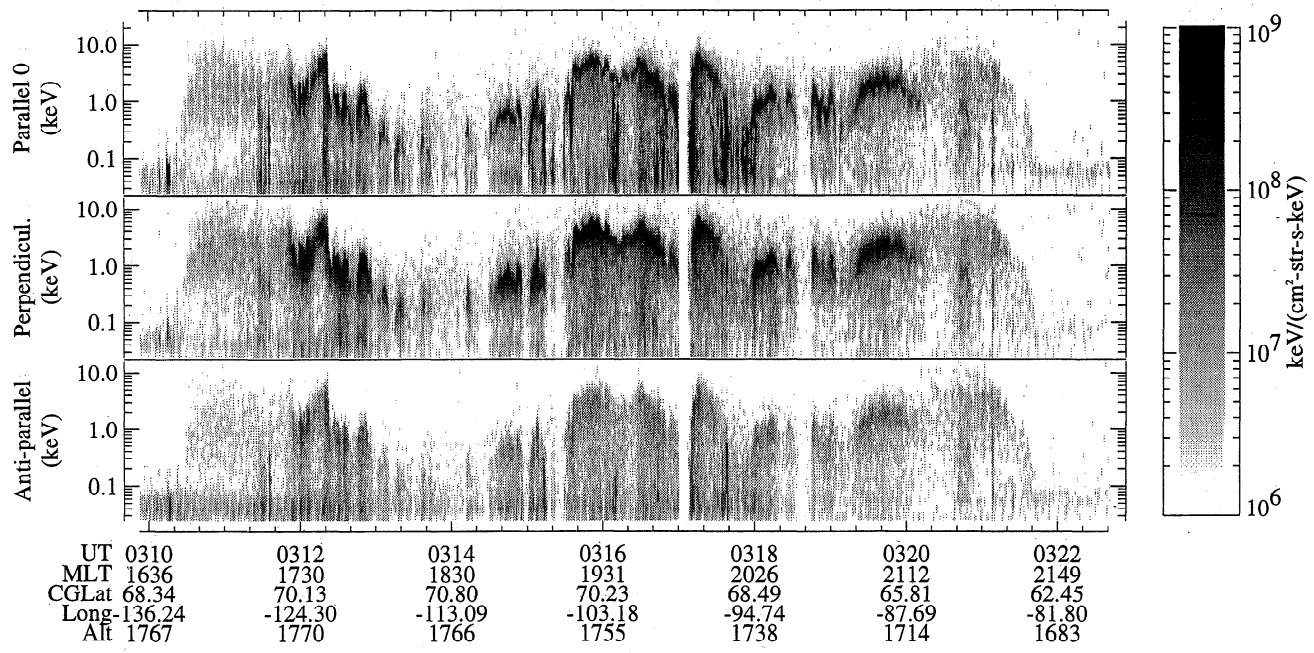

Figure 7. Electron spectrogram for the Freja orbit on March 20.

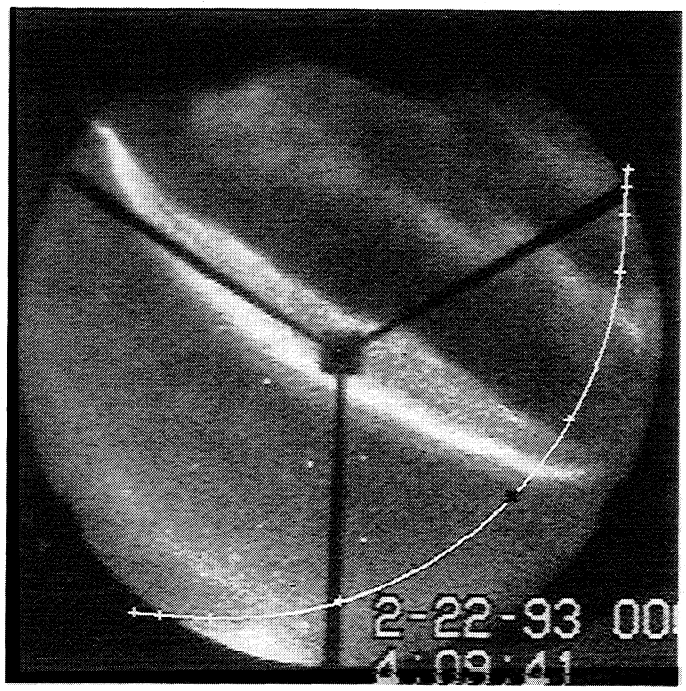

Figure 8. All-sky image taken from Rabbit Lake with the projection of the Freja pass between (bottom left) 0406 and (top right) 0414 UT. Each minute is marked by a plus and the position of Freja with a black asterisk.

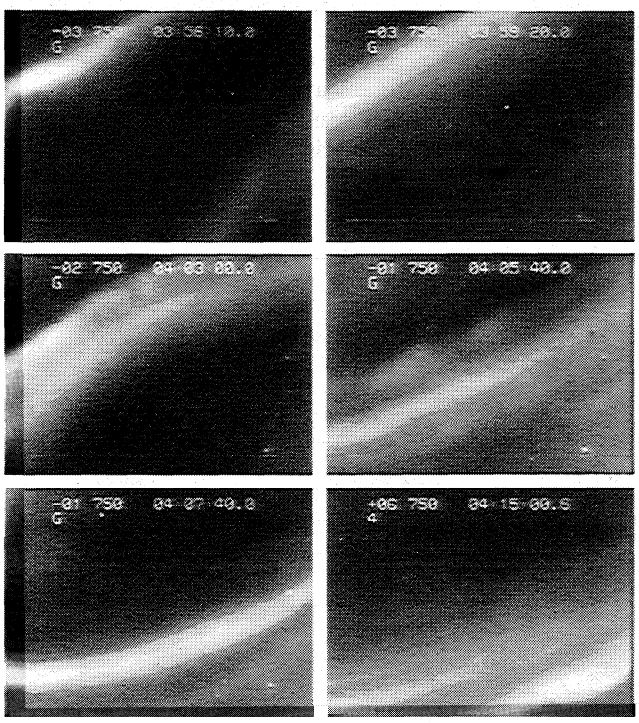

Figure 9. Sequence of CCD camera images taken on February 22 between 0356:10 and 0415:00 UT. The integration times of the images are 5 ms, 5 ms, 10 ms, 20 ms, 20 ms, and 2.56 s. The last image was taken with a 427.8-nm interference filter, and all other images in white light. The north and east directions point to the top and to the left, respectively.

and moved to the south (130 m/s) until it stopped at 0412:50 UT and again increased brightness. There is some indication of a decrease of altitude with increasing brightness but this decrease is within the range of uncertainty of altitude determination. After 0414:10 UT the brightness of the arc decreased and it moved further south.

From 0408 till 0410 UT there were several brightness patterns moving along the fourth arc. While between

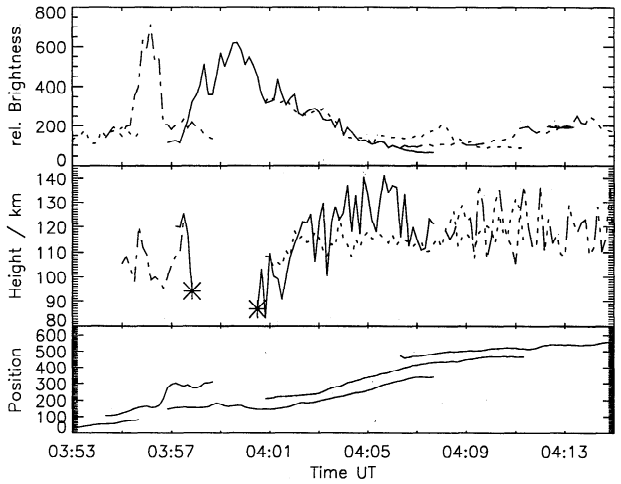

Figure 10. Summary of relative brightness, altitude of maximum light emission, and relative pixel position within the images of the arcs visible on February 22, 1993.

0408 and 0408:40 UT only patterns moving westward with velocities from 3.1 up to 3.6 km/s could be identified, while between 0409 and 0409:40 UT westward motions between 1.5 and 2.3 km/s and eastward motions between 1.0 and 2.3 km/s could be determined.

The fifth and fourth arcs were passed by Freja west of Gillam between 0409:40 and 0409:57 UT and between 0410:16 and 0410:51 UT, respectively. They represent current sheets of 95 and 150 km thickness (not shown).

Again, there was a situation similar to that of March 20. The Gillam area was influenced by the eastward electrojet with its center south of Gillam, and an arc further north was connected to the region between the eastward and the westward electrojet.

From 0405 till 0415 UT Freja measured electric fields pointing mostly northeast at ionospheric level (Figure 11). South of the main arc and between the two arcs the largest fields of 80-110 mV/m were measured, and due to enhanced ionospheric conductivity the field decreased inside of the arcs to 25 mV/m. The BARS radar measured plasma drifts of only 400-500 m/s corresponding to electric fields of about 20 mV/m at ionospheric level.

4. Discussion

The intensities in our images were converted into the brightness of the aurora. We used the theory of *Rees and Luckey* [1974] and examined the 557.7/427.8 ratio under the assumption that the peak energy of the precipitating electrons did not change during the time of the Freja measurement (Table 1). Furthermore, the altitude of the arcs was triangulated during the Freja passes (Table 2). For March 20 and February 22 the altitudes correspond very well to theoretical predictions while on March 18 the high electron peak energy would result in much lower altitudes than measured. The reason for this difference is probably the substorm, and will be discussed later.

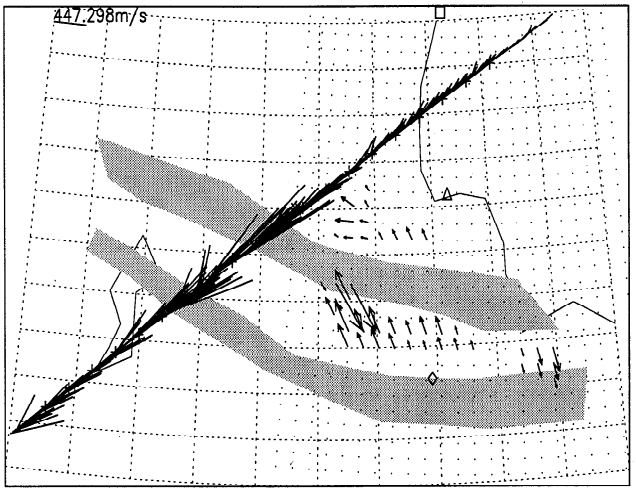

Figure 11. Projection of the electric fields measured by Freja down to ionospheric altitude together with the plasma flow vectors measured by the BARS radar at 0410:30 UT on February 22.

Table 1. Arc Brightness at Different Wavelength Measured Before or After the Pass of Freja

Date	UT	Brightness, kR		557.7/427.8	
		427.8	557.7	Ratio	Theory
Mar. 20	0312	1.1	5.0	4.5	4.0
	0332	0.84	3.1	3.7	4.0
Mar. 18	0412	3.8	10.0	2.6	2.7
Feb. 22	0414	1.1	4.6	4.1	3.4

The theoretical ratios are determined according to *Rees and Luckey*, [1974].

Taking into account the uncertainties of the theory, the calibration, the peak electron energy, and the time differences of about 4-10 s between observations at different wavelengths, we find a close correspondence between experimental and theoretical results. This supports the reliability of the brightness and altitude conversion method [*Rees and Luckey*, 1974; *Kaila*, 1989]. Therefore the intensity in our images along the conjugate points of Freja (Figure 1) could be converted into absolute brightness (Figure 12 [*Haerendel et al.*, 1994]). The electron flux measured along the Freja pass showed small fluctuations within the inverted-V event of up to 25 % which could very nicely be seen in the optical data as well.

The maximum brightnesses at 557.7 nm during the Freja passes were 15.2, 3.5, and 2.6 kR, respectively. Though some individual electron energy spectra on March 18 showed peak energies as high as 25 keV, a much better value is the mean peak energy of 18 keV determined with a 1-s average. In contrast to the earlier work [*Haerendel et al.*, 1994] this value is used in Table 2, but the results do not differ significantly. Taking into account the peak electron energies measured by Freja and the mapping along the dipole field these brightnesses convert into energy fluxes at Freja altitude which correspond well to the satellite measurements.

According to the kinetic theory of the impedance caused by the mirror force acting on hot magnetospheric electrons as current carriers [*Knight*, 1973; *Fridman and Lemaire*, 1980; *Lyons*, 1980] the field-aligned current density in the ionosphere $j_\parallel$ created by an isotropic Maxwellian electron distribution with density n_e and thermal energy E_{th} coming from above into a region of field-aligned potential difference $\phi_\parallel$ (acceleration or energy conversion region), can be expressed by

$$j_\parallel = en_e\sqrt{\frac{E_{th}}{2\pi m_e}}\frac{B_I}{B_M}\cdot \left[1-\left(1-\frac{B_M}{B_I}\right)\exp\left\{-\frac{e\phi_\parallel}{E_{th}(B_I/B_M-1)}\right\}\right]$$
$$\approx e^2 n_e\sqrt{\frac{1}{2\pi m_e E_{th}}}\phi_\parallel = K\phi_\parallel \qquad (3)$$

For $E_{th} \ll e\phi_\parallel \ll E_{th}(B_I/B_M - 1)$ this expression simplifies to a linear relation between the current density and the potential drop with the field-aligned con-

Table 2. Summary of Ground-Based and Satellite-Measured Data During the Freja Passes Over the Inverted-V Auroral Arcs

Date	Observed				Deduced		
	H, km	$\phi_\parallel$, kV	$j_\parallel$, $\mu A/m^2$	$\dot{\varepsilon}_\parallel$, mW/m^2	$\phi_\parallel$ (4) kV	K (3) $\Omega^{-1}m^{-2}$	K (4) $\Omega^{-1}m^{-2}$
March 18, 1993							
Freja		18	0.42	7.0	16.7	9.6×10^{-11}	9.9×10^{-11}
Optical	104 ± 5			8.4	20.0		8.6×10^{-11}
March 20, 1993							
Freja		2.0	0.54	1.6	2.9	1.1×10^{-9}	7.8×10^{-10}
Optical	126 ± 10			1.25	2.3		9.7×10^{-10}
February 22, 1993							
Freja		4.5	0.63	1.4	3.9	5.7×10^{-10}	3.8×10^{-10}
Optical	116 ± 7			1.6	3.5		5.4×10^{-10}

ductance K. Standard values $E_{th} = 500$ eV and $n_e = 0.5\ cm^{-3}$ yield $K = 6.0 \cdot 10^{-10}\ \Omega^{-1}m^{-2}$ [*Borovsky*, 1993]. This value is within the experimentally [*Lyons et al*, 1979; *Sakanoi et al.*, 1995] and theoretically [*Fridman and Lemaire*, 1980] confirmed range of $10^{-9} - 10^{-10}\ \Omega^{-1}m^{-2}$. The parallel potential creates the energy flux $\dot{\varepsilon}$ carried by the accelerated electrons

$$\dot{\varepsilon} = j_\parallel \phi_\parallel = K \phi_\parallel^2. \quad (4)$$

The current density measured by Freja and the energy flux both measured by Freja and calculated from the ground-based optical observation have been used to calculate the parallel potential drop (Equation (4), Table 2) with consideration of the mapping along the dipole field.

All the calculated quantities are in good agreement with the theoretical predictions except the conductance of the event on March 18 which is one order of magnitude too small. Analyzing data of the DE 1 spacecraft, *Marshall et al.* [1991] found similar discrepancies of the linear proportionality between parallel potential and current density. They explained it with variations of density and Maxwellian temperature in the source region. *Sakanoi et al.* [1995] explained similar discrepancies with the possibility that magnetospheric electrons carry only part of the upward field-aligned current. A careful examination of the high energy slope of the auroral electron spectra from March 18 showed a much larger initial thermal electron energy of about (2-3) keV for the incident electron distribution. Taking this value and calculating the electron density in the source region with (3) gives $n_e = 0.1\ cm^{-3}$. The reason for this large discrepancy and for the difference between measured and expected altitude of maximum auroral emission seems to be the magnetospheric substorm which started some minutes before the satellite measurement. Analyzing AMPTE/IRM measurements in the plasma sheet, *Baumjohann et al.* [1991] reported an increase of the ion bulk speed and a decrease of the plasma density during the expansion phase of substorms which may explain our discrepancies. Another reason for our discrepancy may be that the incident electron population can not be represented by an isotropic Maxwellian which is required for (3) [*Lyons*, 1980] or that our procedure underestimated the current density within the inhomogeneous current sheet. Furthermore, *Sakanoi et al.* [1995] showed that the calculated electron densities may scatter over 2 orders of magnitude with a mean value of about $0.1\ cm^{-3}$. Thus, generally, our experimental results support the kinetic theory of the mirror force if we allow for changes of density and energy of the source region electrons during several phases of magnetospheric substorms [*Olsson et al.*, 1996].

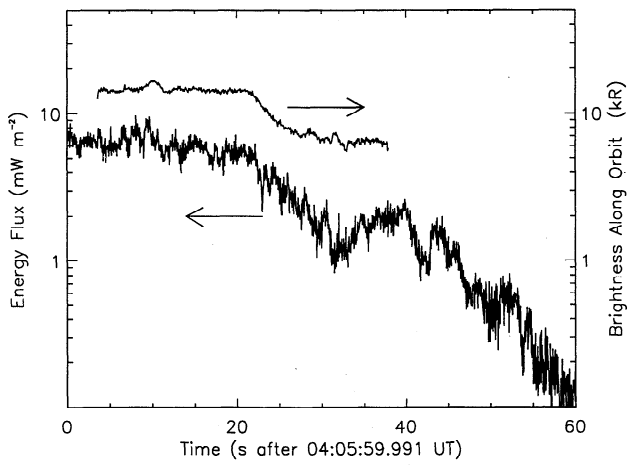

Figure 12. Auroral brightness at 557.7 nm along the track of Freja through the field of view of the MPE CCD camera and electron energy flux simultaneously measured by the satellite.

On February 22 we determined a current system situation which is common to evening auroral arcs [*Marklund et al.*, 1982]. An intense downward current sheet ($1.4\ \mu A/m^2$) which is probably created by up-streaming cold electrons with energies of less than 50 eV is located just equatorward of the arc. This current is connected to the upward current over the arc with a current concentration to the arc edges. Current continuity across the arc is preserved by a polarization electric field which reduces the total electric field within the arc as confirmed by the radar measurements (Figure

11). Within the overall eastward electrojet situation this corresponds to the anti-correlation arc type discussed by *Marklund* [1984]. Adding the knowledge of the southward motion of the arc summarizes the situation as propagation of the arc into the interior of the current system and thus, reducing size and energy content of the ionosphere/magnetosphere system [*Frey et al.*, 1996b].

Even if the flux-time spectrograms show the signature of inverted-V arcs and the observation of a counterflow of brightness patterns on the poleward and equatorward edge of the arcs may be interpreted with inward pointing electric fields, we do not observe these fields at Freja altitude. Thus our observations do not fit the current system for a pure inverted-V arc as it is given by *Marklund* [1984] with opposing electric fields in the E layer. We rather interpret this counterflow with real plasma motions at much higher altitudes, which are shielded from the lower ionosphere by the parallel potential drop in the acceleration region. This interpretation supports the explanation of a superposition of a modified inverted-V with the polarization-dominated electric field pattern [*Marklund*, 1984].

On March 20 as well as on February 22 we saw the counterflow of fine structures within the arcs. Because of the limited extent of our field of view in north-south direction (125 km at 100 km altitude) we could only observe the westward motion in the equatorward part of the arc on March 18. The velocities of these motions would correspond to $\mathbf{E} \times \mathbf{B}$ drifts due to electric fields of 65-140 mV/m (March 18), 35-75 mV/m (March 20), and 50-180 mV/m (February 22). At these times the BARS radar did not measure electric fields of more than 25 mV/m in the vicinity of the arcs. We conclude that the fine-structures are not really frozen in the ionospheric plasma.

One interesting result of the dynamics of the arcs on February 22 is the fact that we find either motion of the arcs with unchanged brightness or brightening without motion. There are two possible explanations. Either the source region of the field aligned current can only supply more energy (which means brightening due to increase of energy or current) under a quite stable situation. Or the relative motion between plasma frame and arc connected field aligned current can be stopped with increased energy input. The appearance of new arcs at a fixed distance in the direction of motion (26–34 km) and with equal brightness adds further experimental evidence to support that conclusion. Earlier observations together with the EISCAT radar [*Frey et al.*, 1996b] showed a general trend of arc motion in the $\mathbf{E} \times \mathbf{B}$ direction of the ambient field but with different speed. *Davis* [1978] discussed three different types of auroral arc motion: (1) movement of the entire flux tube due to $\mathbf{E} \times \mathbf{B}$ drift, (2) tipping of flux tubes when field aligned current alters orientation, and (3) successive dumping. Our observations fit the last explanation that the precipitation is coming from one flux tube at one time and from a different nearby flux tube shortly later. Thus these observations support the idea of successive appearance of precipitation in a new flux tube as a result of the formation of a new inverted-V structure probably

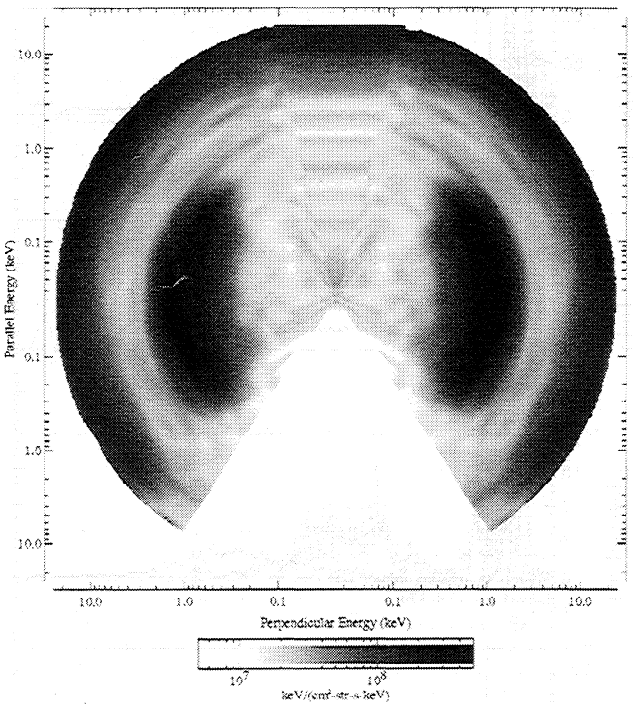

Figure 13. Electron distribution function measured on March 18, 1993, within the broad inverted-V.

created by the interference of Alfvén waves [*Haerendel*, 1983] or by the interaction of changes in the ionospheric conductivity with the magnetosphere [*Lysak*, 1986].

On March 18 we see a substructure within the broad inverted-V passed by Freja (Figure 2). All channels measure the inverted-V structure of electrons with energies as high as 25 keV, but only in the perpendicular channel we do see another inverted-V structure with electron energies between 500 eV and 2 keV (Figure 13). Obviously, these electrons are the remainder of an "older" inverted-V structure and are now trapped between this region with their mirror point in the converging magnetic field and the high-altitude region with the electric potential of the inverted-V [*Eliasson et al.*, 1979]. Furthermore, there are "hot spots" of high electron number flux in the field aligned channels, sometimes with a very narrow energy distribution (Figure 2 at 0405:10 and 0405:30 UT). These electrons can not be accelerated in or above the broad inverted-V acceleration region, because their energy is generally lower than the inverted-V peak energy. These electrons must have been accelerated between the satellite altitude and the inverted-V acceleration region at about 1 R_E.

The perpendicular electric and magnetic field perturbations can be used to determine if the field-aligned currents are mainly closed by ionospheric Pedersen currents

$$\frac{\Delta E_\perp}{\Delta B_\perp} = \frac{1}{\mu_0 \Sigma_p} \tag{5}$$

with the ionospheric Pedersen conductivity Σ_p or by ion polarization currents with shear Alfvén waves

$$\frac{\Delta E_\perp}{\Delta B_\perp} = v_A = \frac{B}{\sqrt{\mu \varrho}} \tag{6}$$

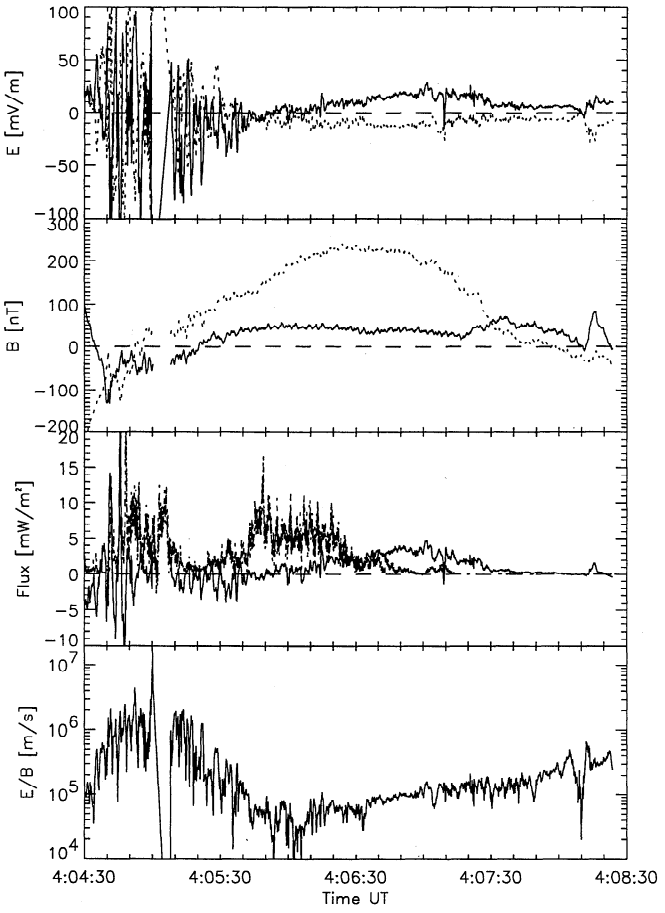

Figure 14. Perpendicular northward (solid line) and eastward (dotted line) electric (top panel) and magnetic (second panel) field at Freja altitude, calculated Poynting electromagnetic energy flux (solid line) and measured electron energy flux (dotted line, third panel) and the quotient of perpendicular electric and magnetic field (lowest panel) for the observation on March 18.

with the Alfvén velocity v_A and the plasma density ϱ [*Dubinin et al.,* 1990; *Ishii et al.,* 1992]. Additionally, it is possible to calculate the electromagnetic energy flux of the Poynting vector **S**

$$\mathbf{S} = \frac{1}{\mu_0}\mathbf{E}_\perp \times \mathbf{B}_\perp. \qquad (7)$$

Since we were interested in the small-scale fluctuations any obvious DC level of the electric field which represents the large-scale magnetospheric controlled structures was subtracted. Two main conclusions can be drawn from the results in Figures 14 - 16.

The transient regions of the flow reversal are controlled by shear Alfvén waves with velocities of $1-5\times 10^6$ m/s and peak velocities of more than 1×10^7 m/s. The mean plasma density calculated from the Langmuir probe data of Freja is $2.0\cdot 10^9\ m^{-3}$. With a mean molecular weight of 3-4 kg/kmol (U.S. Standard Atmosphere, 1976) this gives an Alfvén velocity of 7×10^6 m/s, in good correspondence with the calculated values. In these regions the energy input is mainly carried by Alfvén waves. Two mechanisms can accelerate electrons of the cold ionospheric background up to several keV and create the dynamic arcs observed in the northern part of the all-sky images. Either the Alfvén waves generate secondary high-frequency plasma waves which then accelerate the electrons, or Alfvén waves with a finite perpendicular wave vector produce a parallel electric field in the wave pulse and accelerate the electrons directly [*Goertz,* 1981; *Borovsky,* 1993]. Evidence of wave acceleration above the Freja altitude are the burst-like and strong field aligned electron energy distributions over a large energy interval, as e.g. shown in Figure 2 at 0405:10 and 0405:30 UT, strong electric field fluctuations, and the very small Pedersen conductivities of 0.05-0.4 S.

Within the inverted-V's the main energy carrier between the acceleration region and the ionosphere are the electrostatically accelerated electrons, and the currents are closed in the ionosphere with Pedersen conductivities of 10-30 S, corresponding to E/B values of $2.6-8\times 10^4$ m/s, which are reasonable values within auroral arcs [*Lyons,* 1980]. Generally, the plasma densities measured within the regions of the inverted-V's are slightly higher than in the flow reversal regions with $2-4\times 10^9$ m^{-3} and the Alfvén velocities of $5-7\times 10^6$ m/s are much higher than the values calculated from the electric and magnetic field data of 10^4-10^5 m/s. The thickness of the inverted-V's between 95 km and 200 km corresponds to the scale size region of 64-256

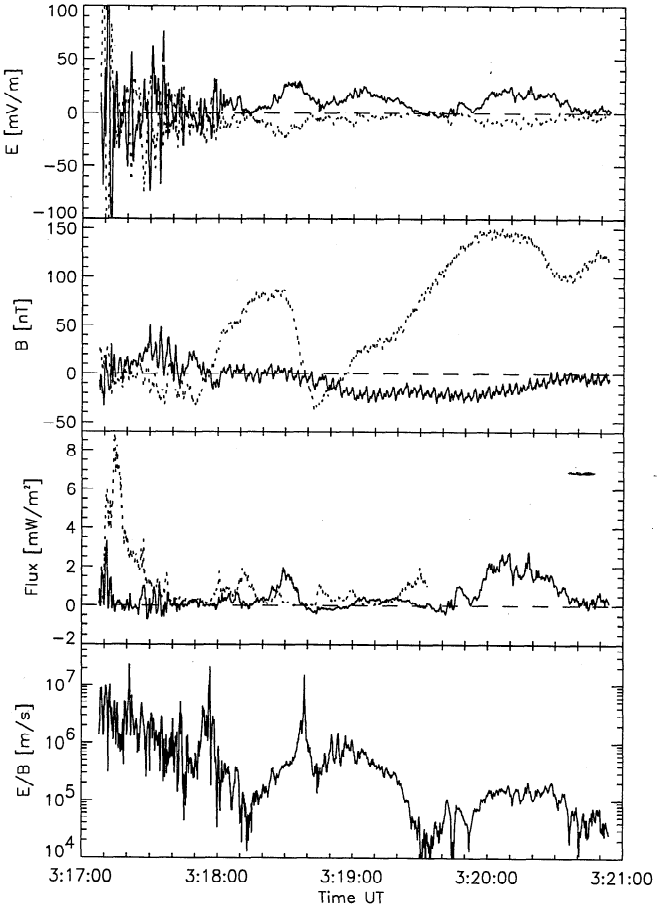

Figure 15. Same as Figure 14 but for March 20.

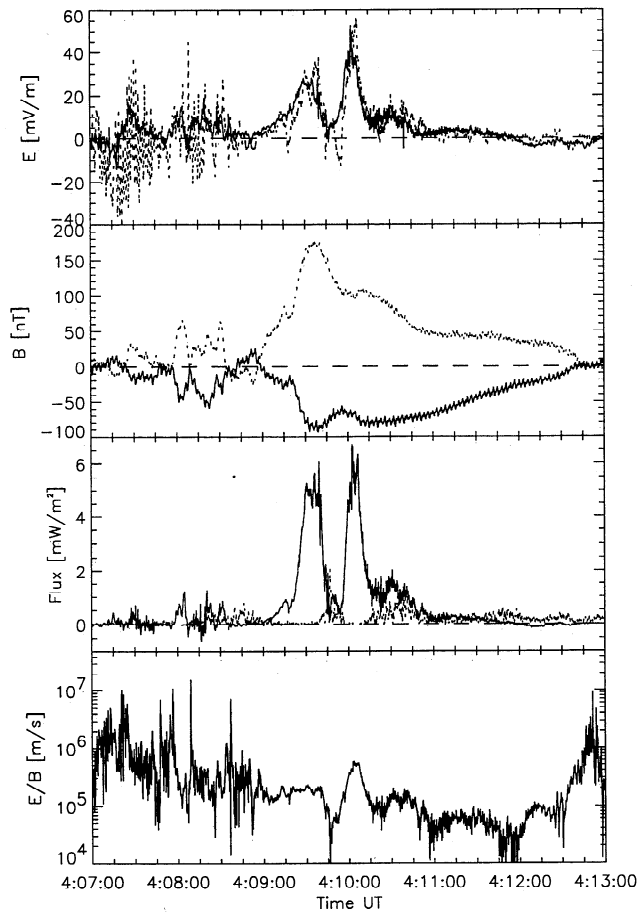

Figure 16. Same as Figure 14 but for February 22.

km determined by [*Ishii et al.*, 1992] as the region for dominating static structures.

5. Conclusions

The coordinated observation of inverted-V type auroral arcs from the ground and by the Freja satellite enabled detailed comparison of optical with electron and field data. One observation is that inverted-V type auroral arcs show a slowly changing optical signature though motions of internal brightness structures represent velocities as high as several kilometers per second. However, these motions are not created by ionospheric electric fields pointing into the structure but are created by high-altitude fields shielded from the ionosphere by the parallel potential drop in the acceleration region.

The motion perpendicular to the elongation of an auroral arc needs not to be a motion with a roughly constant velocity but may well be a mixture between motion of the arc and successive splitting and creation of a new parallel arc. The interesting result of this analysis is that the motion stops during increasing arc brightness and decreasing altitude of maximum light emission and the velocity increases again with decreasing arc brightness and increasing altitude.

Out of three events two may be regarded as a good example for the validity of the linear current-voltage relationship and a constant field-aligned conductivity caused by the mirror force. However, one event shortly after the onset of a magnetospheric substorm may only be explained if drastic changes of the typical parameters for the electron source region density and temperature are excepted. However, even in this inverted-V the magnetospheric-ionospheric coupling via an electrostatic electron acceleration is still controlled by the ionosphere.

Acknowledgments. The authors are grateful to D. McEwen, University of Saskatchewan for providing the Rabbit Lake all-sky images. The German participation in the Freja satellite mission was supported through grant 50 OM 90028 by the Deutsche Agentur für Raumfahrtangelegenheiten (DARA). The CANOPUS Network was constructed and is maintained and operated by the Canadian Space Agency. The Editor thanks two referees for their assistance in evaluating this paper.

References

Baumjohann, W., G. Paschmann, T. Nagai, and H. Lühr, Superposed epoch analysis of the substorm plasma sheet, *J. Geophys. Res.96,* 11605–11608, 1991.

Bochm, M. H., G. Paschmann, J. Clemmons, G. Haerendel, L. Eliasson, and R. Lundin, Freja observations of narrow inverted-V electron precipitation by the two-dimensional electron spectrometer, *Geophys. Res. Lett.21,* 1895–1898, 1994a.

Boehm, M., et al., The TESP electron spectrometer and correlator (F7) on Freja, *Space Sci. Rev., 70,* 509–540, 1994b.

Borovsky, J. E., Auroral arc thicknesses as predicted by various theories, *J. Geophys. Res.98,* 6101–6138, 1993.

Chiu, Y. T., J. M. Cornwall, F. J. Fennell, D. J. Gorney, and P. F. Mizera, Auroral plasmas in the evening sector: Satellite observations and theoretical interpretations, *Space Sci. Rev., 35,* 211–257, 1983.

Davis, T. N., Observed characteristics of auroral forms, *Space Sci. Rev., 22,* 77–113, 1978.

Dubinin, E. M., P. L. Israelevich, and N. S. Nikolaeva, Auroral electro magnetic disturbances at an altitude of 900 km: The relationship between the electric and magnetic field variations, *Planet. Space Sci., 38,* 97–108, 1990.

Eliasson, L., L. Holmgren, and K. Rönnmark, Pitch angle and energy distribution of auroral electrons measured by the ESRO 4 satellite, *Planet. Space Sci., 27,* 87–97, 1979.

Frank, L. A., and K. L. Ackerson, Observations of charged particle precipitation into the auroral zone, *J. Geophys. Res., 76,* 3612–3643, 1971.

Frey, H. U., G. Haerendel, D. Knudsen, S. Buchert, and O. H. Bauer, Optical and radar observations of the motion of auroral arcs, *J. Atmos. Terr. Phys.58,* 57–69, 1996a.

Frey, H. U., G. Haerendel, J. Clemmons, D. D. Wallis, J. Vogt, O. H. Bauer, E. Rieger, M. H. Boehm, and H. Lühr, Studies of auroral arcs using Freja satellite and ground-based data, *Adv. Space Sci., 18, 8,* 107–110, 1996b.

Frey, H. U., W. Lieb, O.H. Bauer, H. Höfner, and G. Haerendel, CCD-camera system for stereoscopic optical observations of the aurora, *SPIE Proc. 2863,* 460–466, 1996c.

Fridman, M., and J. Lemaire, Relationship between auroral electrons fluxes and field aligned electric potential differences, *J. Geophys. Res.85,* 664–670, 1980.

Fung, S.F., and R.A. Hoffman, Finite geometry effects of field-aligned currents, *J. Geophys. Res., 97,* 8569-8579, 1992.

Goertz, C. K., Discrete breakup arcs and kinetic Alfvén waves, in *Physics of Auroral Arc Formation*, Geophys. Monogr. Ser., Vol. 25, edited by S. I. Akasofu and J. R. Kan, AGU, Washington, D.C., 1981.

Grant, I. F., D. R. McDiarmid, and A. G. McNamara, A class of high-m pulsations and its auroral radar signature, *J. Geophys. Res.97,* 8439–8451, 1992.

Gurnett, D. A., Electric field and plasma observations in the magnetosphere, in *Critical Problems of Magnetospheric Physics*, edited by E. R. Dyer, pp. 123–136, Natl. Acad. Sci., Washington, D.C., 1972.

Gurnett, D. A., and L. A. Frank, Observed relationship between electric fields and auroral particle precipitation, *J. Geophys. Res.78,* 145–170, 1973.

Haerendel, G., Alfvén wave model of auroral arcs, in *High-Latitude Space Plasma Physics,* edited by B. Hultqvist and T. Hagfors, pp. 515-535, Plenum, New York, 1983.

Haerendel, G., S. Buchert, C. La Hoz, B. Raaf, and E. Rieger, On the proper motion of auroral arcs, *J. Geophys. Res.98,* 6087–6099, 1993.

Haerendel, G., H. U. Frey, O. H. Bauer, E. Rieger, J. Clemmons, M. H. Boehm, D. D. Wallis, and H. Lühr, Inverted-V events simultaneously observed with the Freja satellite and from ground, *Geophys. Res. Lett.21,* 1891–1894, 1994.

Ishii, M., M. Sugiura, T. Iyemori, and J. A. Slavin, Correlation between magnetic and electric field perturbations in the field-aligned current regions deduced from DE 2 observations, *J. Geophys. Res.97,* 13877–13887, 1992.

Kaila, K.U., Determination of the energy of auroral electrons by the measurement of the emission ratio and altitude of aurorae, *Planet. Space Sci., 37,* 341–349, 1989.

Knight, S., Parallel electric fields, *Planet. Space Sci., 21,* 741–750, 1973.

Lyons, L. R., D. S. Evans, and R. Lundin, An observed relation between magnetic field aligned electric fields and downward electron energy fluxes in the vicinity of auroral forms, *J. Geophys. Res.84,* 457–461, 1979.

Lyons, L. R., Generation of large-scale regions of auroral currents, electric potentials, and precipitation by the divergence of the convection electric field, *J. Geophys. Res., 85,* 17–24, 1980.

Lysak, R. L., Coupling of the dynamic ionosphere to auroral flux tubes, *J. Geophys. Res.91,* 7047–7056, 1986.

Marklund, G., I. Sandahl, and H. Opgenoorth, A study of the dynamics of a discrete auroral arc, *Planet. Space Sci., 30,* 179–197, 1982.

Marklund, G., Auroral arc classification scheme based on the observed arc-associated electric field pattern, *Planet. Space Sci., 32,* 193–211, 1984.

Marklund, G. T., L. G. Blomberg, P.-A. Lindqvist, C.-G. Fälthammar, G. Haerendel, F. Mozer, A. Pedersen, and P. Tanskanen, The double probe electric field experiment on Freja: Experiment description and first results, *Space Sci. Rev., 70,* 483–508, 1994.

Marshall, J. A., J. L. Burch, J. R. Kan, P. H. Reiff, and J. A. Slavin, Sources of field-aligned currents in the auroral plasma, *Geophys. Res. Lett.18,* 45–48, 1991.

McFadden, J. P., C. W. Carlson, and M. H. Boehm, Structure of an energetic narrow discrete arc, *J. Geophys. Res., 95,* 6533–6547, 1990.

Mozer, F. S., C. A. Cattell, M. K. Hudson, R. L. Lysak, M. Temerin, and R. B. Torbert, Satellite measurements and theories of low altitude auroral particle acceleration, *Space Sci. Rev., 27,* 155–167, 1980.

Olsson, A., A. I. Eriksson and P. Janhunen, On the current-voltage relationship in auroral breakups and westward traveling surges, *Ann. Geophys.,* 1265–1273, 1996.

Rees, M. H., and D. Luckey, Auroral electron energy derived from ratio of spectroscopic emissions, 1, Model computations, *J. Geophys. Res.79,* 5181–5186, 1974.

Sakanoi, T., H. Fukunishi, and T. Mukai, Relationship between field-aligned currents and inverted-V parallel potential drops observed at midaltitudes, *J. Geophys. Res.100,* 19343–19360, 1995.

Sonnerup, B. U. O., and L. J. Cahill, Magnetopause structure and attitude from Explorer 12 observations, *J. Geophys. Res.72,* 171–183, 1967.

Zanetti, L. J., et al., Freja Magnetic Field Experiment Team, Magnetic field experiment on the Freja satellite, *Space Sci. Rev., 70,* 465–482, 1994.

O. H. Bauer, G. Haerendel, J. Vogt, Max-Planck-Institut für Extraterrestrische Physik, D-85740 Garching, Germany.

L. Blomberg, Division of Plasma Physics, Alfvén Laboratory, Royal Institute of Technology, S-10044 Stockholm, Sweden.

M. H. Boehm, Lockheed Martin Palo Alto Research Lab, 3251 Hanover St., Palo Alto, CA 94304-1191.

J. H. Clemmons, NASA Goddard Space Flight Center, Mail Code 696, Greenbelt, MD 20771.

H. U. Frey, Space Sciences Laboratory, University of California, Berkeley, CA 94720-7450, (e-mail hfrey@ssl.berkeley.edu).

H. Lühr, GeoForschungszentrum Potsdam, Telegrafenberg, D-14473 Potsdam, Germany.

D. D. Wallis, Hertzberg Institute of Astrophysics, NRC, 100 Sussex Drive, Ottawa, Canada K1A 0R6.

(Received August 30, 1996; revised July 30, 1997; accepted August 2, 1997.)